Quaternary stress regime change in the Hatay region (SE Turkey)

Semir Över, Ulvi Can Ünlügenç, Olivier Bellier

Quaternary stress regime change in the Hatay region (SE Turkey)

Semir Över,[1] Ulvi Can Ünlügenç[2] and Olivier Bellier[3]
[1]*Cumhuriyet University, Department of Geology,* 58140, *Sivas-Turkey. E-mail: Over@cumhuriyet.edu.tr*
[2]*Çukurova University, Department of Geology,* 01100, *Balcaly, Adana-Turkey*
[3]*CEREGE—UMR CNRS 6635—Université Aix-Marseille III, BP 80, Europôle Méditerranéen de l'Arbois*-13545 *Aix en Provence Cedex 4, France*

SUMMARY

In this study we determine the Plio-Quaternary to present-day stress regime acting in the Hatay region located at the northeastern corner of the East Mediterranean region. The modern state of stress is obtained from inversion of focal mechanism solutions of shallow earthquakes. This inversion identifies a dominantly extensional stress regime with a NE-trending σ_{Hmin} (σ_3) axis at the present-day. The stress regime determined from inversion of slip-vectors measured on fault planes confirms that this regime is extensional in the studied area. Both the kinematics and chronologies of fault slip-vectors show that the stress state changed from an earlier strike-slip regime to a younger extensional stress regime with a consistent NE-trending σ_{Hmin}(σ_3) axis. The change from strike-slip to extensional stress regimes probably occurred during the Quaternary. Regionally, both stress regimes induce sinistral displacement on the East Anatolian Fault and Dead Sea Fault systems.

The North Anatolian Fault (NAF) is a dextral strike-slip fault which runs about 1400 km from east to west and has been active since collision between the Eurasian and Arabian plates. Together with the sinistral East Anatolian fault, the NAF intracontinental deformation zone contributes to the westward extrusion of Anatolia as a consequence of northward drift of Arabia. Consequently, the Late Cenozoic stress regimes acting in the Hatay region result from the coeval influence of forces due to: (1) the subduction processes in the west and southwest; (2) the continental collision in the east, and (3) the westward escape of the Anatolian Block. However, the timing of the temporal stress transition suggests that the Quaternary stress regime change resulted from subduction processes with the extensional stress regime in the Hatay region being mainly attributable to roll-back of the Mediterranean subducted slab along the Cyprus Arc.

Key words: eastern Mediterranean domain, fault slip-vector inversion, quaternary stress regime, strike-slip/extension tectonics.

INTRODUCTION

The study area, shown in Fig. 1, lies in an intersection domain between three active belts: the southern end of the left-lateral East Anatolian Fault (EAF), the northern end of the left-lateral Dead Sea Fault (DSF) and the Cyprus Arc. This domain accommodates the relative motions of Arabia/Anatolia, Africa/Arabia and Anatolia/Africa respectively (McKenzie 1972, 1978; Le Pichon & Angelier 1979; Sengör 1979; Jackson & McKenzie 1984; Dewey *et al.* 1986; Westaway 1994). The EAF is approximately 500 km long and runs southwestward from Karliova in eastern Anatolia, where it joins the North Anatolian Fault (NAF), either to the Gulf of Iskenderun (Jackson & McKenzie 1984, 1988) or to the town of Antakya (Arpat & Saroglu 1972; Perinçek & Çemen 1990; Saroglu *et al.* 1992). Fig. 2 shows SPOT XS (K/J; 118/277) imagery of the study area. The NAF is a dextral strike-slip fault which runs about 1400 km from east to west, bounding the north of the Anatolian Block. It appears to have been active since the collision between the Eurasian and Arabian plates. The NAF, intracontinental deformation zone, contributes with the sinistral East Anatolian Fault to the westward extrusion of Anatolia resulting from the northward drift of Arabia.

Left-lateral displacement on the EAF has been characterized from seismological observations (McKenzie 1972; Jackson & McKenzie 1984; Taymaz *et al.* 1991) and structural studies (Arpat & Saroglu 1975; Saroglu *et al.* 1992). Thus, the major fault seems to run through the Amanos mountains from Turkoglu to Antakya (Perinçek & Çemen 1990; Saroglu *et al.* 1992). This segment, with NNE–SSW (N15° ± 5) orientation is about 145 km long and is known as the Amanos (Lyberis *et al.* 1992) or Karasu Fault (Westaway 1994). This NNE-trending fault segment bounds the western flank of the ∼30-km wide Amik Basin, filled with Plio-Quaternary sediments (Lyberis *et al.* 1992) to a thickness of more than 1000 m (Perinçek &

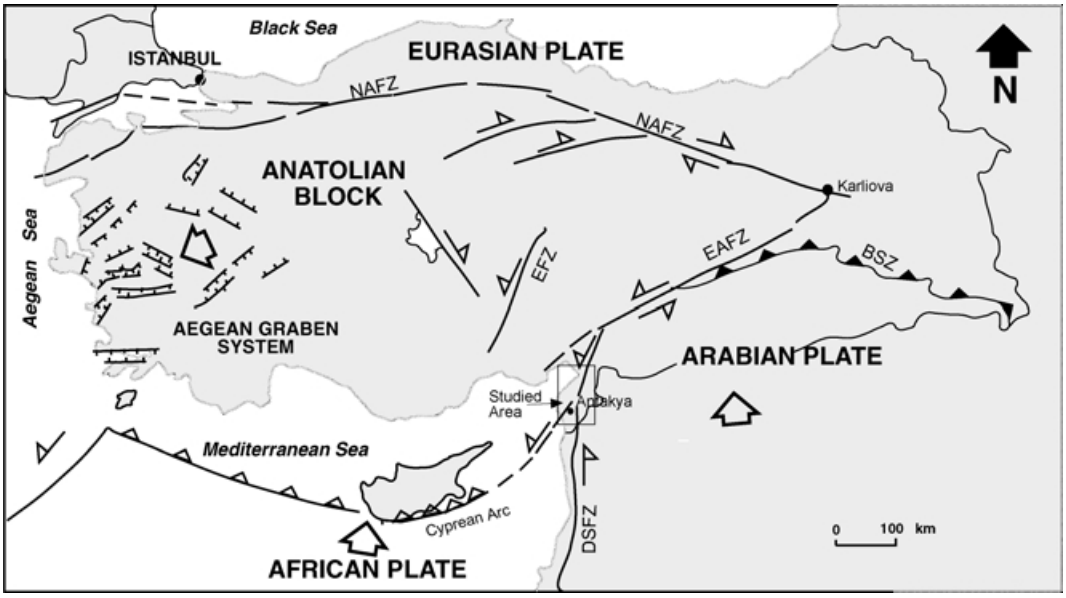

Figure 1. Sketch map of the eastern Mediterranean tectonic framework (modified after Sengör 1979; Gürsoy *et al.* 1998).

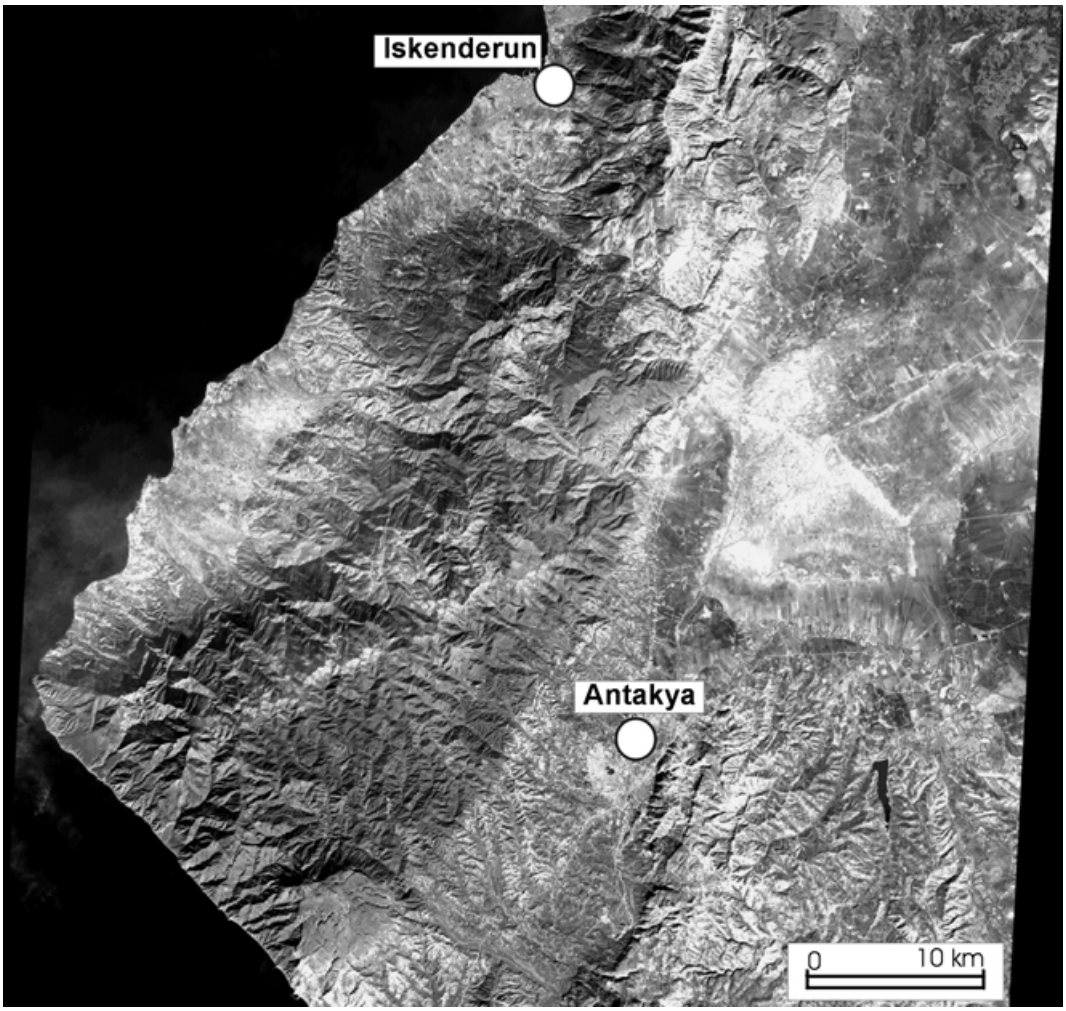

Figure 2. SPOT XS imagery (K/J, 118/277) covering the kinematic study area.

Eren 1990). The K–Ar, Nd, Sr and Pb isotopic dating studies yield a Quaternary to recent age for the basaltic rocks along the Karasu Valley (Capan *et al.* 1987; Rojay *et al.* 2001).

The differential northward motion of Arabia with respect to Africa is essentially taken up by the DSF, which is approximately 1000 km long and extends northwards from the Red Sea to Antakya (Lyberis *et al.* 1992). This fault has generally been interpreted as a left-lateral strike-slip fault system (Nur & Ben-Avraham 1978; Lovelock 1984; Mart & Rabinowitz 1986; Hempton 1987). The plate boundary between southern Anatolia and the Africa Plates is a subduction zone comprising the Hellenic and Cyprus arcs. The deformation style along the Cyprus Arc and its prolongation up to the Hatay region has been discussed by a number of authors. Most (i.e., McKenzie 1970, 1972; Ben-Meneham *et al.* 1976, 1988; Kempler & Garfunkel 1994; Mart & Woodside 1994) believe that the arc and its continental extension as a dominantly strike-slip fault seem to constitute a transform plate boundary. Thus, the Hatay region appears to experience the coeval influence of the kinematics of the major active belts of the eastern Mediterranean region namely the EAF, DSF and Cyprus Arc, in relation to northward drift of Afro-Arabian plate as the Anatolian Block moves westward.

Although the East Mediterranean region is characterized by a wide zone of orogenesis, and despite a century of active studies (see discussion in Ambraseys 1965, 1970; McKenzie 1972, 1978; Ben-Meneham *et al.* 1976, 1988; Jackson & McKenzie 1984, 1988; Westaway & Arger 1996), the fault kinematics and stress regime of the Anatolian domain are still poorly known, particularly in the southeastern part. The present knowledge of Cenozoic stress regimes mainly concerns the western domain of Anatolia (e.g. Angelier *et al.* 1981; Hancock & Barka 1987; Zanchi & Angelier 1993) and the North Anatolian Fault Zone (Bellier *et al.* 1997; Over *et al.* 1997). Fault kinematic analysis and earthquake slip vectors provide evidence for a recent temporal change in stress state along the NAF (Bellier *et al.* 1997; Over *et al.* 1997). From correlation with the recent temporal change, which has occurred in the Aegean domain, Mercier *et al.* (1979, 1989) and Bellier *et al.* (1997) attribute this NAF temporal change in stress regime to the Aegean subduction process, i.e., variation in slab force, along the Hellenic Arc. The fault kinematic studies, which have been carried out around the Amik Basin (Lyberis *et al.* 1992) indicate that two stress state regimes; a strike-slip regime and a NE–SW extension are recorded here. The authors interpret these different stress regimes to a coeval spatial variation. To complement the knowledge of stress regimes, we have studied the recent stress regime changes in the area surrounding Antakya. The Late Cenozoic stress states are provided by inversion of slip-vectors measured on minor and major fault planes which affect Miocene to Plio-Quaternary deposits as well as undifferentiated Eocene limestones. The present-day stress field acting in the Hatay region is determined from inversion of the focal mechanisms of major earthquakes.

GEODYNAMIC SETTING

The active deformation in the eastern Mediterranean region, particularly in Anatolia, has occurred as a result of the differential continental collision between Afro-Arabian and the Eurasian plates since the Late Miocene following closure of the Bitlis oceanic basin. This basin was formerly part of the Neotethys and corresponds to the Bitlis Suture (Sengör *et al.* 1985). The northward convergence of Arabia produces thickening of the crust in eastern Turkey and compressional deformation along the Bitlis–Zagros fold and thrust belt (Saroglu & Yilmaz 1990) (Fig. 1). Contemporaneously, this northward motion with respect to Eurasia, gives rise to the westward extrusion of the Anatolian Block along the dextral NAF and sinistral EAF (McKenzie 1972; Tapponnier 1977; Sengör *et al.* 1985; Dewey *et al.* 1986) these faults constitute the northern and eastern boundaries of the Anatolia Block respectively. Northward motion of the African Plate results in subduction in the Eastern Mediterranean along both the Hellenic and Cyprus arcs (McKenzie 1972; Rotstein & Ben-Avraham 1985; DeMets *et al.* 1990; Barka & Reilinger 1997). There is a controversy regarding the nature of subduction along the Cyprus Arc which is delineated as a plate boundary (Ben-Meneham *et al.* 1976, 1988; Biju-Duval *et al.* 1978; Büyükasıkoglu 1980; Jackson & McKenzie 1984; Kempler & Garfunkel 1994; Mart & Woodside 1994; Barka & Reilinger 1997). In both arcs, subduction has been documented by bathymetric and seismic data complemented by earthquake study (Rabinowitz & Ryan 1970; McKenzie 1970, 1972; Papazachos 1973). From Seismic refraction data Markis (1981) found that the Mediterranean crust near Cyprus is oceanic. A seismicity study in the Eastern Mediterranean to the east of Cyprus shows a zone dipping approximately northwards demonstrating that the plate consumption, as in Hellenic Arc, appears to be achieved through subduction of oceanic lithosphere beneath Anatolia (Rotstein & Kafka 1982). This is in agreement with the earthquake focal mechanisms that provide evidence for the thrusting process along the south of Cyprus (Büyükasıkoglu 1980). The subduction segmentation is responsible for the tectonic regime patterns in the overriding Anatolian crust (Barka & Reilinger 1997). Global models (DeMets *et al.* 1990) suggest that the Hellenic Trench is moving southwards relative to Europe as consequence of roll-back of the Mediterranean subducted slab to produce extensional tectonics in the overriding plate, i.e., in the Aegean domain and western Anatolia (Mercier *et al.* 1979, 1989; Le Pichon 1982; Sorel *et al.* 1988). The structural kinematic analysis suggests a variation of deformation style between compression and extension and confirms the existence of local extension in the overriding plate. This is observed north of Cyprus in the Adana and Cilicia Basins (Kempler & Garfunkel 1994). The extensional tectonics is attributed to roll-back of the Mediterranean subducted slab along the Cyprus Arc (Robertson *et al.* 1991), as it is similarly observed along the Hellenic Arc. In addition, the slab retreat is inferred to be a dominant control on crustal extension i.e., a decrease of the horizontal stress on the overriding plate which has been noted along the Hellenic Arc (Mercier *et al.* 1979, 1989; Le Pichon & Angelier 1981), in the Andean Cordillera (Mercier 1981), and along the Eolian arcs (Malinverno & Ryan 1986).

SEISMICITY AND SEISMOTECTONICS WITHIN THE HATAY DOMAIN

Many authors (Barazangi & Dorman 1969; McKenzie 1972, 1978; Comninakis & Papazachos 1972; Nowroozi 1972; Rotstein & Kafka 1982) have described the general trends of seismicity in the eastern Mediterranean, Anatolia and Levant countries. The region has been characterized by a low seismicity during this century (Jackson & McKenzie 1988). However, it is known to have been seismically active from historical catalogues (Poirier & Taher 1980; Ambraseys & Barazangi 1989). Two large historical earthquakes (shown by star in Fig. 3a) destroyed the town of Antakya on 1822 August 13 $M \cong 7.4$, and on 1872 April 13 $M \cong 7.2$. The distribution of earthquakes of magnitude greater than 4 between 1900 and 1998 occurring in the Hatay region is given in Fig. 3(a). The earthquake data are compiled for a period between 1900–1993 from the International Seismological Center (ISC), the United States Geological Survey (USGS), the

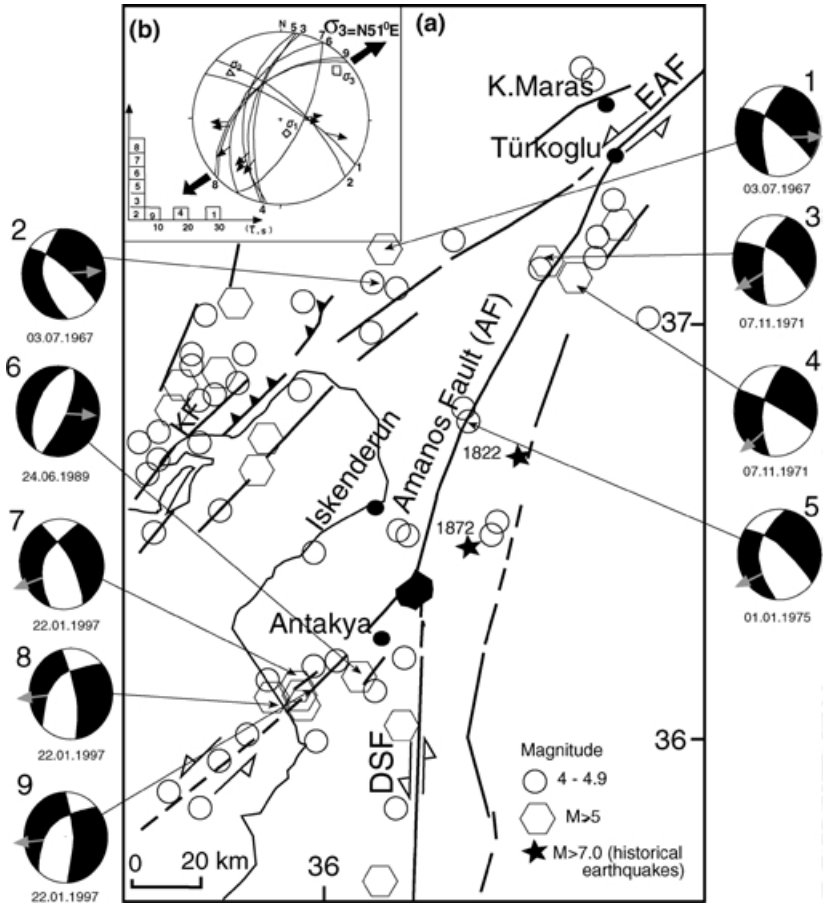

Figure 3. (a) Seismotectonic map of the Hatay region and surroundings and the focal mechanisms of shallow earthquakes (references are given for each earthquake in Table 1). Plots show nodal planes and slip-vector arrows on the preferred seismic fault planes (arrows point in the direction of the horizontal azimuth of the slip vector), the preferred seismic plane are chosen according to the method of Carey-Gailhardis & Mercier (1987). Numbers outside the balloons refer to the focal mechanism labels given in Table 1. KT: Karatas Fault. (b) Lower hemisphere stereoplots of the earthquake slip data with the present-day regional principal stress directions computed from the focal mechanisms of earthquakes shown in (a) and in Table 1. Numbers inside the histogram and outside the stereoplot refer to the focal mechanism labels given in Table 1. Black arrows indicate the σ_3 direction of these extensional stress states. Lower hemisphere plots show fault planes and measured slip-vectors (arrows): arrows point in the direction of the horizontal azimuth of the slip-vector. Stress axes obtained from the inversions are shown by diamonds (σ_1), triangles (σ_2) and square (σ_3). Thick lines on the fault traces give the deviation angle between measured (s) and predicted (τ) slip-vectors on each fault plane. Histogram shows distribution of deviation angles (angle between the observed slip, s, and the predicted slip, τ.

Preliminary Determination of Epicenters (PDE) and the Istanbul Kandilli Observatory and earthquake Research Institute (KOERI) (Demirtas & Yilmaz 1996). The seismic data were complemented by catalogues of KOERI and USGS for the period of 1994–1998. The earthquakes are mainly distributed along the following active structures: (1) SW end of East Anatolian Fault (represented by Karatas Fault zone), (2) southern end of East Anatolian Fault Zone, (represented by Amanos Fault), (3) northern part of Dead Sea Fault Zone, and (4) the Cyprus Arc and its extension on land. These tectonic belts control the seismic activity in the Hatay region and seem to accommodate the regional deformation in relation to the northward movement of the Arabian and African plates with respect to Anatolia, part of which lies within the Eurasian Plate.

FAULT KINEMATIC ANALYSIS

Methodology: Inversion of fault slip data to determine Plio-Quaternary stress state

The kinematics of a fault population are defined using the striations measured on the fault planes at several sites (26 sites in an area of approximately 35×65 km^2). The studied sites of fault slip measurements are shown in Fig. 4 and the location (latitude and longitude) of each site and the age of the faulted formations from which the striae were measured are given in the Table in Appendix 1. The main objective of this work is to define the Mio–Pliocene to present-day states of stress in SE Anatolia and their probable significance in relation to regional tectonic events. The methodology of fault kinematic studies to determine palaeostress fields and demonstrate temporal and spatial changes in late Cenozoic stress states has been used in active tectonic areas around the world over past 20 years (e.g., Angelier *et al.* 1981; Sebrier *et al.* 1988; Mercier *et al.* 1989, 1991; Bellier & Zoback 1995; Bellier *et al.* 1997; Over *et al.* 1997). To determine stress fields responsible for Late Cenozoic deformations in the investigated area, we have carried out a quantitative inversion of distinct families of slip data determined at each individual site, using the method originally proposed by Carey (1979). This inversion method assumes that the slip represented by the striation (s) occurs in the direction of the resolved shear stress (τ) on each fault plane, the fault plane being the pre-existing fracture. Inversion computes a mean best-fitting deviatoric stress tensor from a set of striated faults by minimizing the angular deviation between a predicted slip-vector

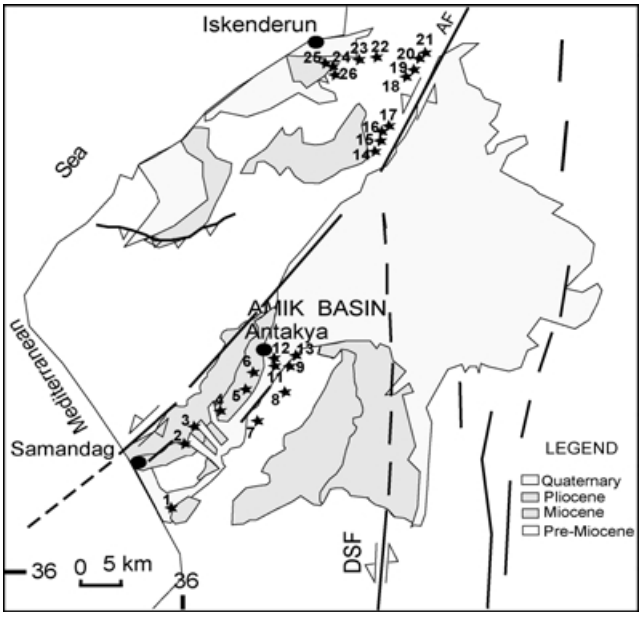

Figure 4. Simplified geological map of Hatay region. Numbers indicate locations of fault-slip measurement sites (see Table A1 of Appendix for latitudes and longitudes).

(maximum shear, τ) and the observed striation (s) (e.g. Carey 1979; Angelier 1984). Similar inversion methodologies, all based on minimization of the 'deviation' angle have been developed by a number of investigators for robust data sets including a wide variety of slip vectors and fault plane orientations (see references in Mercier *et al.* 1991). Inversion results include the orientation (azimuth and plunge) of the principal stress axes of a mean deviatoric stress tensor as well as a 'stress ratio' $R = (\sigma_2 - \sigma_1)/(\sigma_3 - \sigma_1)$. Principal stress axes, σ_1, σ_2 and σ_3, correspond to the compressional, intermediate and extensional deviatoric stress axes, respectively, while the R ratio is a linear quantity describing the relative stress magnitude, where $|\sigma_1| + |\sigma_2| + |\sigma_3| = 0$. As defined, the stress ratio, varies between two end member uniaxial stress states ($R = 0$ when $\sigma_2 = \sigma_1$ and $R = 1$ when $\sigma_2 = \sigma_3$). The results of the stress inversion are generally considered reliable if 80 per cent of the deviation angles (angle between the calculated slip-vector 'τ' and the striation 's') are less than 20°.

Bellier & Zoback (1995) proposed an approach to deal with poorly distributed fault sets (e.g. data sets that contain faults with few distinct strike directions and few dipping in both directions) utilizing a 'fixed' inversion, i.e. one in which the principal stress axes are fixed to lie in horizontal and vertical planes (considered generally to be the case in the Earth's crust, see Zoback & Zoback 1980). For this fixed inversion there are only two unknowns (the orientation of one of the horizontal stresses and the stress ratio) thus requiring only two independent fault sets for a solution. Bellier & Zoback (1995) showed that the inferred horizontal stress orientations from the fixed inversion are generally within 5–10° of the stress axes obtained from poorly constrained full (or standard) inversions although the fixed inversion results may be characterized by unstable and unconstrained R values.

Inversion of seismic slip-vector data sets to determine the Present-day stress state

To compute the state of stress responsible for present-day faulting from the population of focal mechanisms of earthquakes that have occurred in the Hatay region (i.e. between SW Antakya and Turkoglu) we use an inversion method proposed by Carey-Gailhardis & Mercier (1987); this is one of several existing algorithms (Vasseur *et al.* 1983; Gephart & Forsyth 1984). The inversion is a statistical method, which allows calculation of the best mean fitting stress state from a population of focal mechanisms by selecting one of two nodal planes as the seismic fault plane. The selection can be made by using computer analysis or from the co-seismic rupture or from the spatial epicentre distribution of the aftershock sequence. Indeed, one of the focal mechanism solutions (i.e. nodal planes) is the seismic fault slip vector, which is in agreement with the principal stress axes. It is possible to compute the seismic fault slip following the model proposed by Bott (1959). This method requires a knowledge of the seismic slip-vectors and consequently the selection of the preferred seismic fault plane from each couple of nodal planes. This selection is possible by computation: one of the two slip-vectors of a focal solution is the seismic slip vector in agreement with the principal stress axes. For this slip-vector the computed 'stress ratio' defined by the formula $[R = (\sigma_2 - \sigma_1)/(\sigma_3 - \sigma_1)]$ is such that $0 < R < 1$ (Bott 1959). If one of the two nodal planes satisfies these conditions, the other does not satisfy, it unless the two nodal planes intersect each other along a principal stress axis (Carey 1979).

In general, the state of stress obtained from a set of earthquake focal mechanism leads to well-constrained evaluation of the regional stress state in agreement with the state of stress deduced from inversion of striation measurements on fault planes (Mercier *et al.* 1991; Zanchi & Angelier 1993; Bellier *et al.* 1997).

RESULTS

Modern stress field

To define a regionally significant stress tensor responsible for present-day faulting within the investigated area, we have used the inversion method of Carey-Gailhardis & Mercier (1987), applied to the focal mechanisms of shallow earthquakes in the Hatay region. The available focal mechanisms for earthquakes of magnitude 4.7 to 5.5 for a period between 1967–1997 are given in Table 1 and shown in Fig. 3(a). Their slip vectors, reported using stereonets in Fig. 3(a), indicate normal to oblique-slip faulting. Earthquakes with magnitudes between 4.7 and 5.5 can be considered as intermediate magnitude events and therefore, represent the significant present-day stress state acting in this region. The solutions n °6 to 8 correspond to the Antakya earthquake of 22 January 1997 of magnitude $M_b = 5.5$ ($M_w = 5.8$) and its aftershocks of magnitudes $M_b = 5.2$ and 5.3 respectively. The focal mechanism solutions for these events are obtained by rupture process modelling (Erdik *et al.* 1997), based on the body wave inversion method proposed by Kikuchi & Kanamori (1991). These solutions identify predominantly normal faulting mechanisms with a strike-slip component for the main event and its aftershock.

Inversion of earthquake slip vectors gives consistent results for the present-day stress acting in the Hatay region corresponding to a normal faulting stress regime ($\sigma_1 = \sigma_V$) characterized by a N51°E-trending axis (Fig. 3b). It is shown in the following Sections that the present-day stress state determined by inversion of seismic fault-slips agrees with the stress deviator computed from the youngest striae measured on fault planes.

Late Cenozoic stress state change

Fault slip chronologies and inversions of the striae indicate sequential changes in the stress regime. These variations consist

Table 1. Parameters of focal mechanisms of shallow earthquakes occurring in the Hatay region. References: 1. Büyükasykoglu (1980); 2. Osmansahin *et al.* (1986); 3. Harvard CMT catalogues; 4. Erdik *et al.* (1997).

No.	Date	Lat°	Lon°	Planes 1 strike°/dip°	Plane 2 strike°/dip°	T-axis Az/pl	Mag. mb	*h* (km)	Ref
1	Apr. 7 1967	37.43	36.17	192/54	301/70	63/7	5.0 (Ms)	38	1
2	Apr. 7 1967	37.36	36.27	312/64	174/37	352/21	4.9 (Ms)	32	1
3	July 11 1971	37.17	36.71	191/52	304/68	64/9	5.2	9	2
4	July 11 1971	36.12	36.80	189/58	294/70	59/7	5.2	19	1
5	Jan. 1 1975	36.67	36.49	300/65	198/44	58/14	4.8	35	2
6	Jun. 24 1989	36.28	36.13	203/28	27/62	115/17	5.1 (Mw)	15	3
7	Jan. 22 1997	36.23	35.85	208/38	331/68	80/17	5.5	33	4
8	Jan. 22 1997	36.21	35.65	228/42NW	358/62	108/10	5.2	33	4
9	Jan. 22 1997	39.21	35.92	225/43	355/64	108/10	5.3	33	4

successively of strike-slip then normal faulting during the Late Cenozoic that correspond to regionally and/or locally significant stress regimes around the SE boundary of the Anatolian Block. Unfortunately, it is difficult to constrain the ages of the fault. In this study we include results of all measurements obtained in Early Cenozoic to Quaternary age rocks. In general, we have observed more than one set of striae on a fault plane. These distinct data sets can be geologically separated using structural arguments such as the cross-cutting relationships of the striae (see methodology in Mercier *et al.* 1991; Bellier & Zoback 1995). We give in Fig. 5 the fault planes, which contain superimposed slip-vectors measured in several sites. These cross-cutting relationships between striations permit recognition of the Late Cenozoic to Present-day stress regime history.

Faults with normal vertical offsets of ∼0.1–1 m affecting Plio-Quaternary deposits (silt, clay, and sandstone) were observed in the area. An example of these faults is exposed along Antakya–Samandag road (site 3, in Fig. 6, for more precision see Table 1 in Appendix 1) where normal faults displace Plio–Quaternary deposits with a vertical offset of approximately 3.5 metres. A shallow rake strike-slip fault plane (1 on Fig. 6) cut by a younger normal fault plane (2 on Fig. 6) can clearly be seen. The older strike-slip faulting striae agree roughly with NW-oriented compressional and NE-oriented extensional axes discussed in the next section, while the younger wide rakes of the normal faulting slip indicate a NE-trending extensional axis also discussed below.

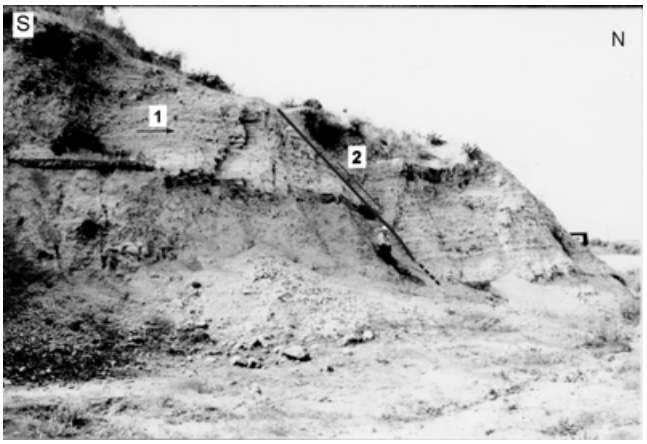

Figure 6. West facing photographic view of Plio-Quaternary deposits at site 3. These fault planes show an example of two distinct stage: the older, strike-slip fault plane, is indicated by number 1, and the younger, normal fault plane, is indicated by number 2.

Strike-slip stress regime

The first Late Miocene to present-day stress regime corresponds to a strike-slip deformation stage affecting the Antakya region. Evidence for this old strike-slip stress regime is recorded by slip-vectors on faults, which affect Miocene and Plio–Quaternary deposits as well as undifferentiated Eocene limestone. The slip data were measured both along major and minor fault planes. Results of the inversion of all the fault slip vector data sets belonging to this deformation stage consistently indicate a strike-slip faulting stress regime with a mean NW-trending maximum horizontal stress ($\sigma_{\mathrm{Hmax}} = \sigma_1$) axis and a NE-trending minimum horizontal stress ($\sigma_{\mathrm{Hmin}} = \sigma_3$) axis (Fig. 7). The inversion results are shown on the lower hemisphere stereoplot and histograms of deviation angles between the observed (s) and predicted (τ) slip direction. The principal deviatoric stresses (azimuth and plunge and magnitude of σ_1, σ_2, σ_3) are also plotted. Individual and combined site σ_1, σ_3 directions are reported on the map of

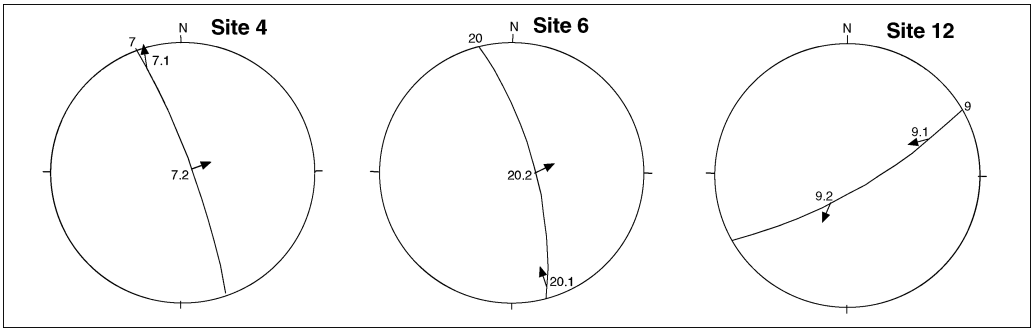

Figure 5. Chronology, e.g., cross-cutting relationship between different families of slip-vectors measured on fault planes at several sites. Fault planes and measured striations (arrows) are shown in a lower hemisphere stereographic projection (Wulf lower hemisphere), arrows point in the horizontal slip azimuth direction. Numbers describe individual fault-plane measurements; the older slip-vector on each fault plane is indicated by (.1) and the younger by (.2). Labels outside to the right of the stereonets refer to sites located in Fig. 4 and listed in the Table A1 of the Appendix.

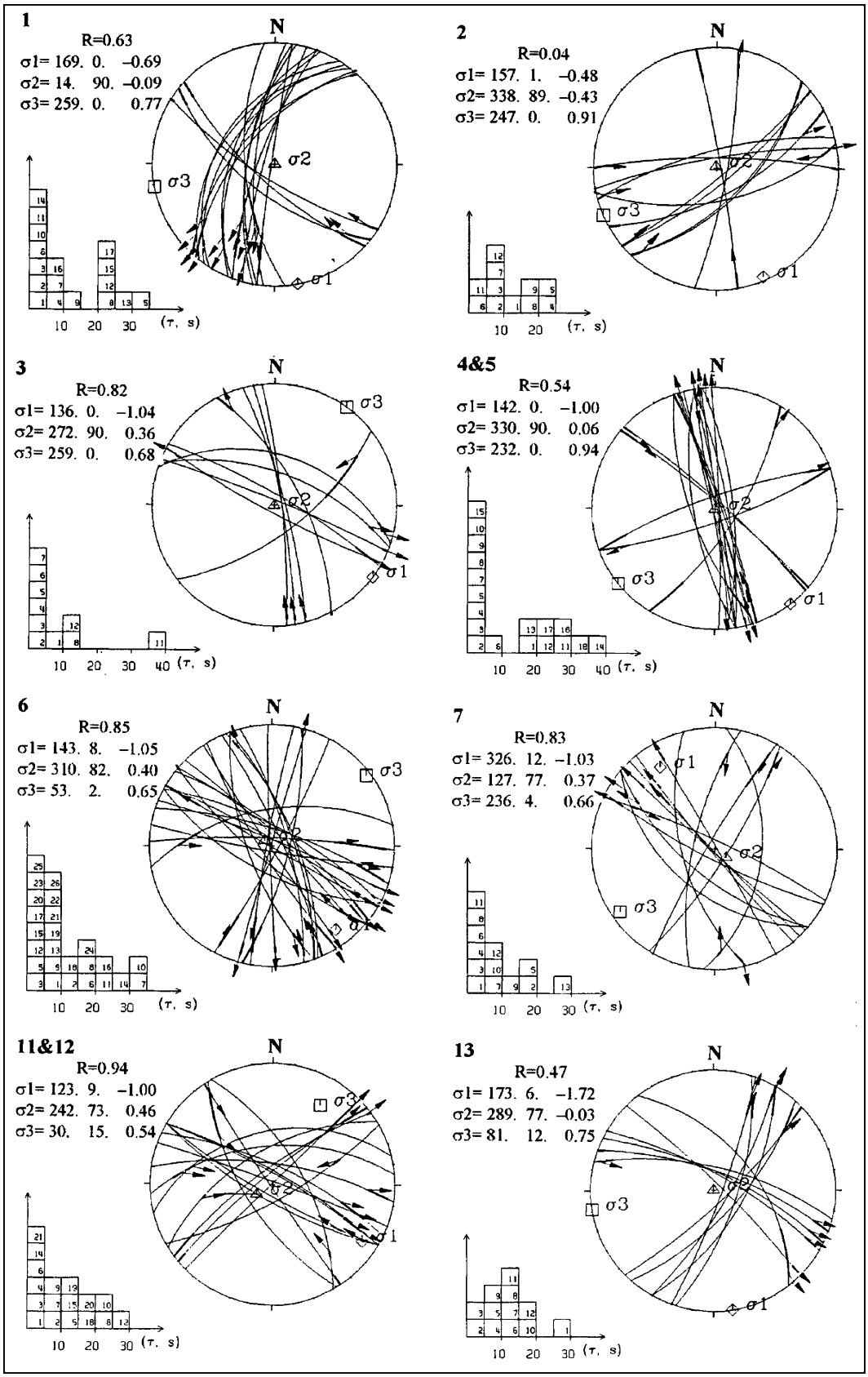

Figure 7. Lower hemisphere stereoplots showing strike-slip faulting data measured in and surrounding Antakya and the results determined by Carey (1979) inversion method, as shown in Table 1 of Appendix 2. Labels outside to the left of the stereonets refer to sites located in Fig. 4 and listed in Table of Appendix 1. The results include deviatoric stress parameters (σ_1, σ_2 and σ_3 axes) determined by Carey (1979) inversion method, that is azimuth, plunge and relative magnitudes of principal axes as well as the stress ratio value [$R = (\sigma_2 - \sigma_1)/(\sigma_3 - \sigma_1)$]. See caption to Fig. 3(b).

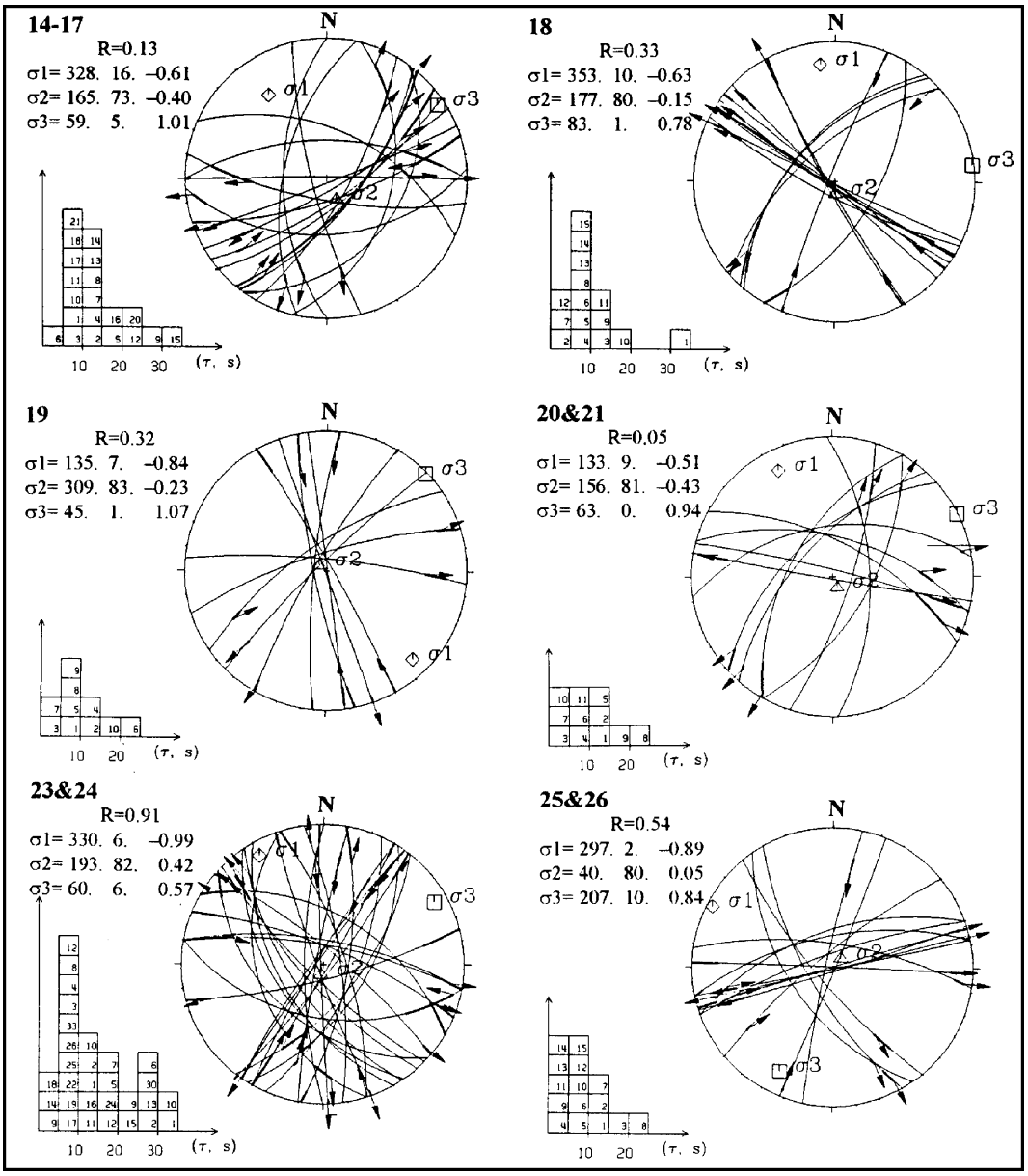

Figure 7. (*Continued.*)

Fig. 8(a). All stress deviators indicate a strike-slip stress regime with a NNW- to WNW-trending σ_{Hmax} (σ_1 axes ranging between N7°W and N63°W) and a NNE- to ENE-trending σ_{Hmin} (σ_3 axes trending between N27°E and N83°E). To constrain the kinematic parameters of this older strike-slip stress regime at regional scale, the major representative planes selected from each fault kinematic site were inverted. The inversion results show a mean representative and stable strike-slip state of stress characterized by a N326°E (N34°W) σ_1 axis and N56°E σ_3 axis (SFmaj1 on Fig. 9a). The strike-slip stress regime with a consistent NW-trending σ_1 and NE-trending σ_3 axes induce left-lateral movement along the Amanos fault i.e. at the southern end of East Anatolian Fault.

Extensional stress regime

The measured normal faulting slip-vectors affect the Quaternary to Miocene deposits as well as undifferentiated Eocene sediments around the Antakya area. The inversion of normal faulting slip data shows two significantly distinct kinematics characterizing NE–SW and approximately E–W extensions respectively. Unfortunately, we do not have any evidence for the relative age of these extensions.

NE-trending extensional stress state

The slip-vectors measured at several sites across the investigated area indicate a normal to oblique slip deformation stage which postdates older strike-slip deformation. One of the significant examples of this deformation is observed along the Antakya–Samandag road at site 3 where we measured only four normal faulting slips, which do not allow us to compute the deviatoric stress tensor. The indicated extensional directions are deduced from field data such as the character of faulting: normal faults (2 in Fig. 6) affect the Plio–Quaternary deposits and displace silt, clay and sandstone series, already deformed by strike-slip faulting (1 in Fig. 6). As shown in Fig. 10(a), the inversions of these data consistently indicate a normal faulting stress regime with a NE-trending σ_3. Lower hemisphere stereoplots of all fault kinematics and inversion results (for sites with sufficient data to calculate stress deviators), histograms of deviation

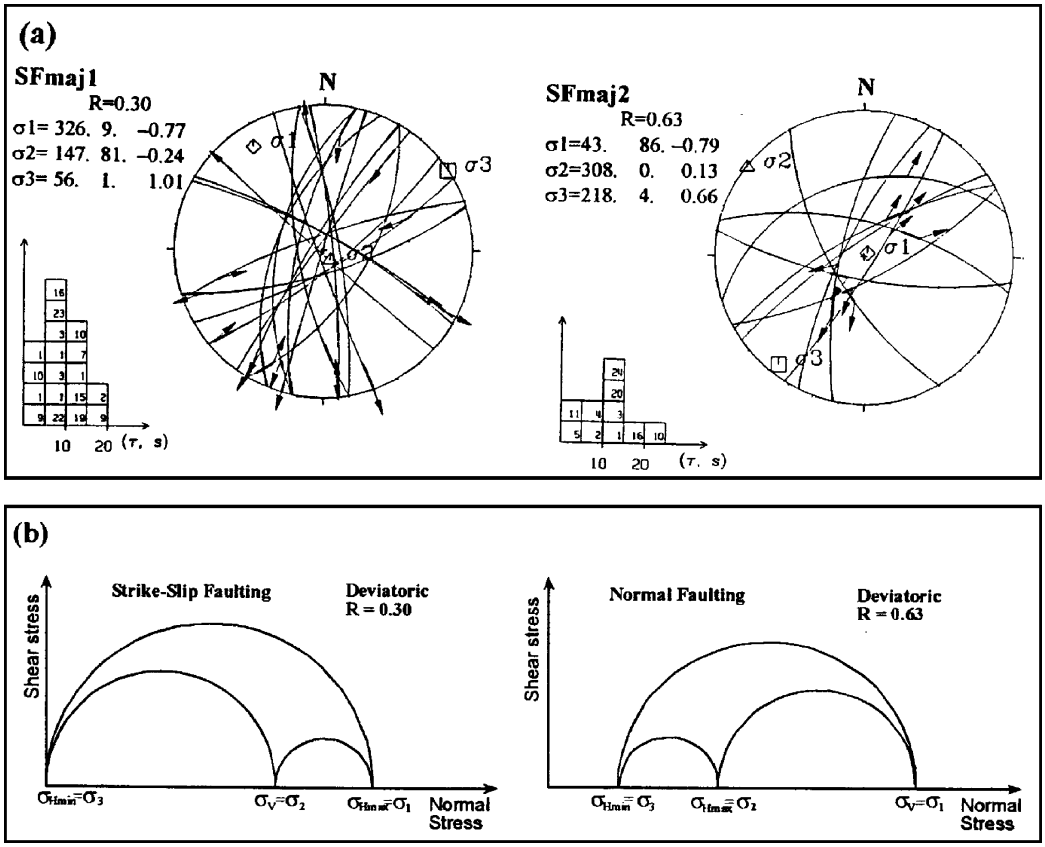

Figure 8. (a) Lower hemisphere stereoplots showing the inversion results of selected major and/or representative fault planes of strike-slip and extensional stress regimes respectively. (b) Mohr's circle representations of coaxial stress states for two regional strike-slip and normal faulting regimes. For two stress regimes the minimum horizontal stress (σ_{Hmin}) is NE-trending σ_3 and the vertical stress is given by σ_v (equals in the strike-slip σ_2 case and σ_1 in the normal faulting case).

angles (τ,s) and the principal stress axes are plotted in Fig. 10(a). Individual and combined site σ_2, σ_3 directions are reported on the map in Fig. 8(b). All stress deviators indicate a normal faulting stress regime with a NNW- to WNW-trending σ_{Hmax} (σ_2 axes ranging between N23°W and N66°W) and a NNE- to ENE-trending σ_{Hmin} (σ_3 axes trending between N24°E and N67°E). To better constrain the kinematic parameters of this stress state on a regional scale, we have carried out an inversion of the major and/or representative planes selected from each site. This gives a mean representative and stable normal faulting stress regime with a N218°E (N38°E) σ_{Hmin} (σ_3) and a N308°E (N52°W) σ_{Hmax} (σ_2) axes (SFmaj2 on Fig. 9a).

The NE-trending extension evidenced in this study agrees with results of kinematic observations by Perinçek & Çemen (1990); based on study of the seismic reflection profiles. They identify the presence of normal growth faults with southwest extension bounding the Amik Basin. The NE–SW extensional direction produces a transtensional regime comprising normal faulting with a sinistral component on major faults (e.g. NNE-strike Amanos Fault).

E-trending extensional stress state

We have measured normal faulting slip-vectors (sites 8 & 9 and 11 & 12) characterizing another extensional regime with an approximately E-trending σ_3 axis. The data sets for normal faulting at the combined sites 11 & 12 did not allow us to compute the deviatoric stress tensor but extensional directions can be deduced from field data such as the character of faulting. The inversion results are shown on Fig. 10(b). Individual and combined site σ_3 directions are shown on the map of Fig. 9(b). This E-trending extension seems to be subsequent to the regionally significant NE-extension and is probably of only locally significance.

DISCUSSION AND CONCLUSIONS

In the Hatay region, the present-day stress state deduced from inversion of earthquake focal mechanisms is a dominantly normal faulting regime ($\sigma_1 = \sigma_V$) with a small strike-slip component. The trend of present-day extension is NE–SW with a corresponding azimuth of σ_{Hmin} (σ_3) axis of N51°E. It produces normal faulting with a left-lateral component on the major NNE-striking Amanos Fault i.e. at the southern end of the EAF.

The Late Cenozoic tectonics in, and surrounding, the Antakya area is marked by a change from old strike-slip to younger normal faulting stress regimes which reactivated inherited faults and produced new ones. The strike-slip stress regime is characterized by a NW-trending (N34°W) σ_{Hmax} (σ_1) axis and a NE-trending (N56°E) σ_{Hmin} (σ_3) axis, which induced a left-lateral strike-slip movement along both the major faults (i.e. the EAF and DSF). The Late Miocene-Pliocene compressive structures (reverse faults and folds) observed along the Amanos Range to the north of Turkoglu (Kahramanmaras) (Gökçen *et al.* 1986; Lyberis *et al.* 1992; Chorowicz *et al.* 1994) could have been produced or reactivated during this strike-slip stress regime with a consistent NW-trending σ_1 axis, as a consequence of the applied boundary forces, i.e. northward motions of the Arabian plate in the east and of the African

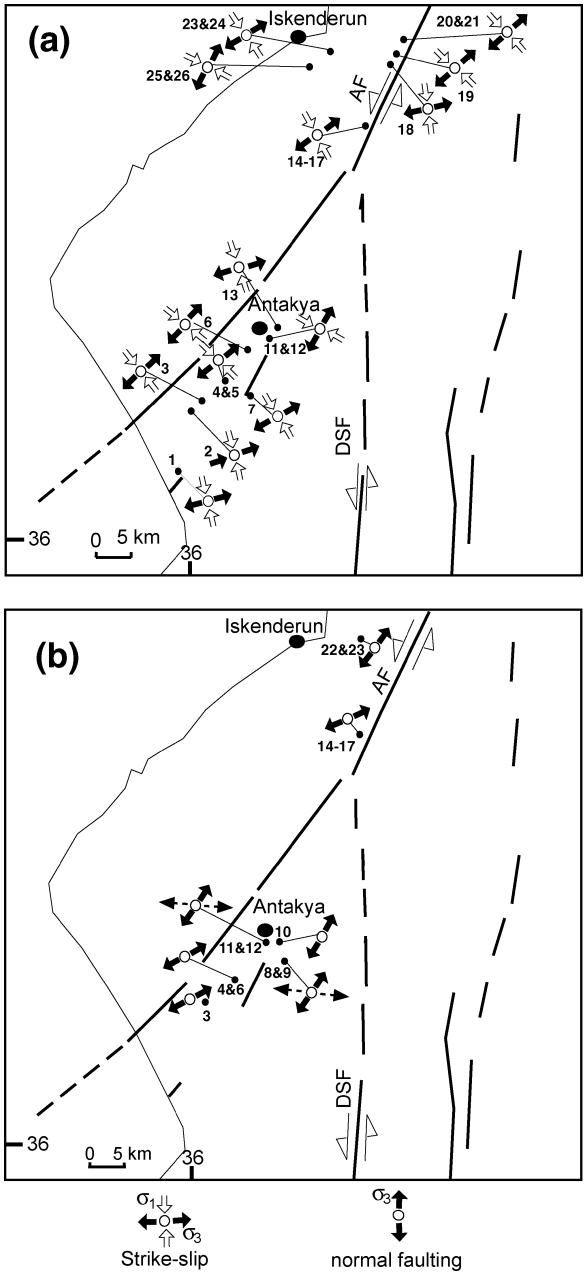

Figure 9. Simplified tectonic map of Hatay region. Azimuths of σ_3 (extensional stress) and s_1 (compressional stress) axes for the Plio-Quaternary stress regimes are shown. Dots show approximate locations of fault-slip measurement sites (identified by numbers); exact site locations are reported in terms of their latitudes and longitudes in the Table of Appendix 1. (a) refers to the strike-slip stress regime deduced from the fault slip. White and black arrows indicate respectively the σ_1 and σ_3 azimuths of the stress states given in Fig. 7 and in Table A2 of the Appendix. (b) refers to the NE-trending extensional stress regime deduced from the fault slip. Black arrows indicate σ_3 azimuths of the stress states plotted Fig. 10(a) and in Table A2(a) of the Appendix. Dashed arrows correspond to σ_3 azimuths of the local normal faulting stress regime given in Fig. 10(b) and Table A2(b) of the Appendix.

plate in the west-southwest (McKenzie 1972; Sengör 1979; Dewey *et al.* 1986; Robertson *et al.* 1991).

The regime change from strike-slip to normal-faulting is characterized by a consistent NE-trending σ_{Hmin} (σ_3) axis and the NE-extensional direction conforms to a global left-lateral displacement along major structures such as the NNE-trending Amanos Fault near the confluence of the EAF and DSF. This change is shown by cross-cutting striae on fault planes and by the fault slip-vector inversions.

Unfortunately, the geological control on the timing of faulting is too poor for us to determine accurately the time of the change in stress state. The volcanism and the Quaternary deposition indicate the youngest extension in the Hatay region (Capan *et al.* 1987; Perinçek & Eren 1990; Yürür & Chorowicz 1998) and this NE-trending extension was probably responsible for the formation of the Amik Basin, filled with Quaternary deposits. Seismic reflection profiles show the presence of normal faults bounding this basin (Perinçek & Çemen 1990) that are consistent with NE–SW extension. The correlation with previous studies allows us to estimate that the normal faulting was contemporaneous with Quaternary deposition. Indeed, the younger slip-vectors recorded by brittle deformation (i.e. striations) and deduced from focal mechanisms of the earthquakes lead us to conclude that the regionally significant Recent to present-day stress regime is extensional but produces a minor strike-slip component along NNE-trending major faults in the Hatay region. This tectonic stress regime seems to extend over a wide area between south of the Amik Basin to the Turkoglu region. Using radar and DEM imagery Chorowicz *et al.* (1999) deduce that the transtension to extension have prevailed since the Neogene over a much larger area including along the NAF in Eastern Anatolia and implying that the lithosphere of Anatolia is subjected to extension. This regional transtensional to extensional stress regime characterized by a SW-trending σ_3 has prevailed since the Pleistocene (Bellier *et al.* 1997). The configuration of the regional transtension to extension observed along the central and eastern NAF is not the response of simple lateral westward extrusion induced by boundary forces of Arabia-Anatolia collision but is rather due to the retreat of the Hellenic slab (Bellier *et al.* 1997; Chorowicz *et al.* 1999).

The observed Plio-Quaternary to Present-day stress regimes are coaxial with a NW-trending σ_{Hmax} (σ_1 in the strike-slip case, σ_2 in the normal faulting case) and a NE-trending σ_{Hmin} (σ_3) axis change in stress regime corresponding only to variation in the horizontal and/or vertical stress magnitudes. Thus, a change from strike-slip faulting stress regime to a normal faulting stress regime, both with a consistent NE-trending σ_{Hmin} (σ_3) axis, can be explained by a decrease in the NW-trending horizontal stress axis (σ_{Hmax}) and/or by an increase in the vertical stress axis (σ_V) (equals σ_2 in the strike-slip case and σ_1 in the normal faulting case). The change between these stress states can be represented on Mohr's circle (Fig. 8b). This representation shows that the change from strike-slip to normal faulting stress regimes corresponds to a temporal decrease the magnitude of σ_{Hmax}. This decrease has produced the extensional/transtensional character of the recent stress regime along the Hatay region.

The source of the variation in horizontal stress magnitude in the overriding plate has resulted from the slab–pull force which has accompanied slab retreat above a subduction zone along the Cyprus Arc (Robertson *et al.* 1991). The change between compressional/uplift to extensional tectonic regimes observed in south-southwest Anatolia (e.g. Robertson *et al.* 1991; Kempler & Garfunkel 1994) can be explained by variations of the Mediterranean slab force from the Mio–Pliocene to the present-day along the Cyprus Arc (Robertson 1990; Robertson *et al.* 1991). The slab-pull force is considered to be a major force in driving the plates and controlling the tectonics of an overriding plate above a subduction zone (Forsyth & Uyeda 1975; Dewey 1980; Carlson & Melia 1984; Sebrier & Soler 1991). The tectonic regimes acting in the Hatay region since the Mio–Pliocene seem to result from the coeval influence of boundary forces due to active Arabia/Anatolia continental collision in the northeast and easternmost Mediterranean subduction

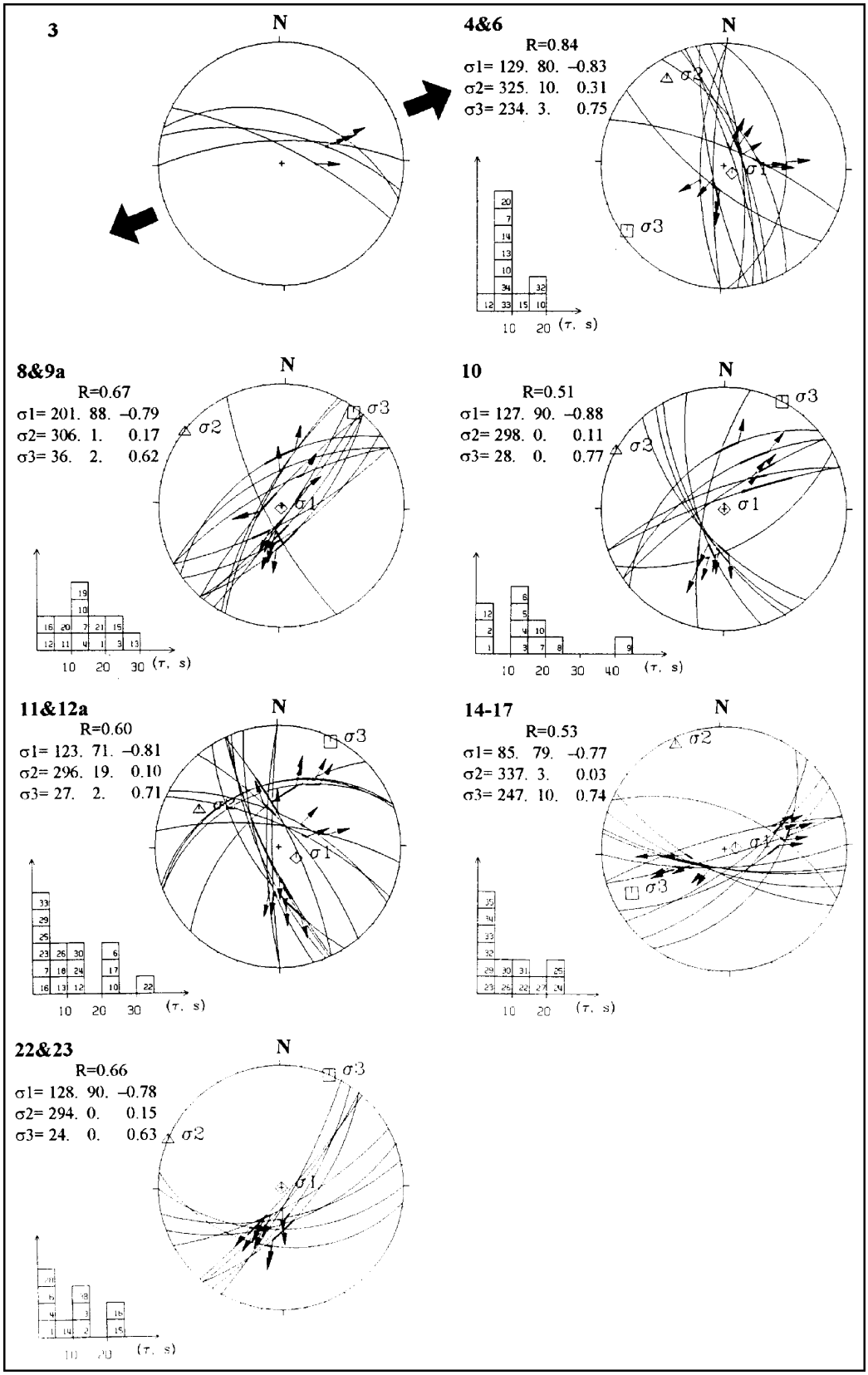

Figure 10. Lower hemisphere stereoplots showing NE-trending normal faulting data measured in and surrounding Antakya and the results determined by Carey (1979) inversion method, as shown in Table 2(a) of Appendix 2. Labels outside to the left of the stereonets refer to sites located in Fig. 4 and listed in Table of Appendix 1. See caption to Figs 3(b) and 7. (b) Lower hemisphere stereoplots showing E-trending normal faulting data measured in and surrounding Antakya and the results determined by Carey (1979) inversion method, as shown in Table A2(b) of the Appendix. Labels outside to the left of the stereonets refer to sites located in Fig. 4 and listed in Table A1. See caption to Figs 3(b) and 7.

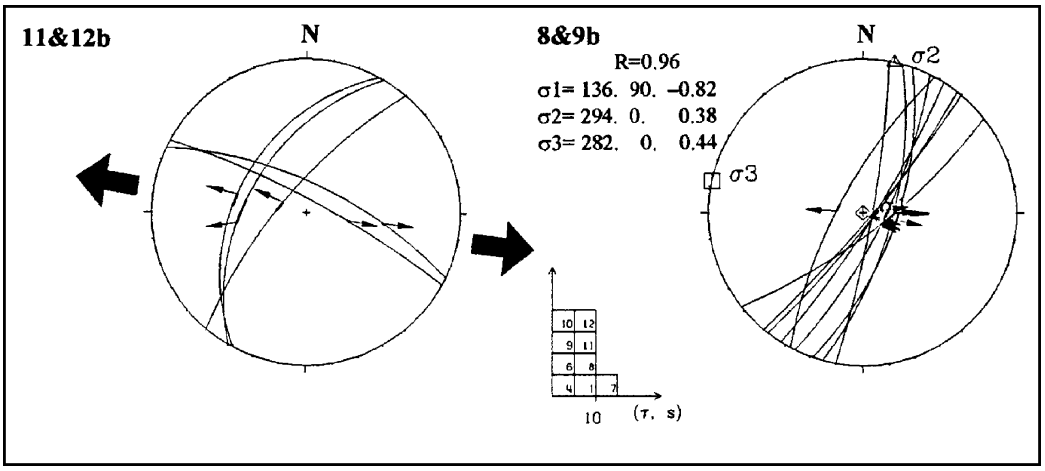

Figure 10. (*Continued.*)

along the Cyprus Arc in the southwest (McKenzie 1972; Sengör 1979; Dewey *et al.* 1986; Robertson *et al.* 1991).

Consequently, the Late Cenozoic stress regimes acting in the Hatay region results from the coeval influence of forces due: (1) the subduction processes, at the west-southwest; (2) the continental collision, at the east, and (3) the westward escape of the Anatolian block. However, the change in the stress regimes evidenced by our data from the Hatay region corresponds to variations in horizontal and/or vertical stress magnitudes probably in relation to geodynamic changes within the easternmost Mediterranean associated with the subducting slab along the Cyprus Arc.

ACKNOWLEDGMENTS

This work was financially supported by Research Foundation of Cumhuriyet University (Project n° M121). The SPOT image was provided thanks to the ISIS program (CNES). Special thanks are due to Prof. Dr N. Türkelli and Dr A. Pinar for helpful comments, reviews and criticisms, that considerably improved the manuscript. We also thank to Dr John D.A. Piper for the revision of the English version. We are grateful to anonymous reviewers for valuable comments and suggestions that largely improved the quality of the manuscript.

REFERENCES

Ambraseys, N.N., 1965. The seismic history of Cyprus, Revue, *Un. int. Secours.,* **3,** 25–48.

Ambraseys, N.N., 1970. Some characteristic features of the Anatolian fault zone, *Tectonophysics,* **9,** 143–165.

Ambraseys, N.N. & Barazangi, M., 1989. The 1759 earthquake in the Bekaa Valley: Implications for earthquake hazard assessment in the eastern Mediterranean region, *J. geophys. Res.,* **94,** 4007–4013.

Angelier, J., Dumont, J.F., Karamanderesi, H., Poisson, A., Simsek, S. & Uysal, S., 1981. Analyse of fault mechanisms and expansion of southwestern Anatolia since the Late Miocene, *Tectonophysics,* **75,** T1–T9.

Angelier, J., 1984. Tectonic analysis of fault slip data sets, *J. geophys. Res.,* **89,** 5835–5848.

Arpat, E. & Saroğlu, F., 1972. The East Anatolian fault system: thoughts on its development, *M.T.A. Bull.,* **78,** 33–39.

Arpat, E. & Saroglu, F., 1975. Some recent tectonic events in Turkey, *Bull. geol. Soc. Turkey,* **18,** 91–101.

Barazangi, M. & Dorman, J., 1969. World seismicity maps compiled from ESSA, Coast and geodetic survey epicenter data1961–1967, *Bull. seism. Soc. Am.,* **59,** 369–380.

Barka, A.A. & Reilinger, R., 1997. Active tectonics of the Mediterranean region: deduced from GPS, neotectonic and seismicity data., *Annali di Geophysica, XI,* **3,** 587–610.

Bellier, O. & Zoback, M., 1995. Recent state of stress change in the Walker Lane zone western basin and Range Province-USA, *Tectonics,* **14,** 564–593.

Bellier, O., Over, S., Poisson, A. & Andrieux, J., 1997. Recent temporal change in the stress state and modern stress field along North Anatolian Fault Zone (Turkey), *Geophys. J. Int.,* **131,** 61–86.

Ben-Avraham, Z., Kempler, D. & Ginzburg, A., 1988. Plate convergence in the Cyprus arc, *Tectonophysics,* **146,** 231–240.

Ben-Meneham, A., Nur, A. & Vered, M., 1976. Tectonic seismicity and structure of the Afro-Eurasian junction, the breaking of an incoherent plate, *Phys. Earth. planet. Inter.,* **12,** 1–50.

Biju-Duval, B., Lapierre, H. & Letouzey, J., 1978. Is the Toros massif (Cyprus) allochtonous? *Bull. Soc. Geol. Fr.,* **18,** 1347–1356.

Bott, M.H.P., 1959. The mechanism of oblique slip faulting, *Geol. Mag.,* **96,** 109–117.

Büyükasıkoglu, S., 1980. Sismolojik verilere göre dogu akdenizin kuzeyinde ve güneydogu Anadolu'da Avrasya-Afrika levha sınırlarının özellikleri (in Turkish), *Bull. Earthq. Res. Inst.,* Ministry of Reconstruction and Resettlement, **29,** 58–74.

Capan, U.Z., Vidal, P. & Cantagrel, J.M., 1987. K-Ar, Nd, Sr and Pb isotopic study of the Quaternary volcanism in Karasu Valley (Hatay), N-end of Dead Sea reft zone in SE Turkey, *Yerbilimleri,* **14,** 165–178.

Carey, E., 1979. Recherche des directions principales de contraintes associées au jeu d'une population de failles, *Rev. Géol. Dynam. Géog. Phys.,* **21,** 57–66.

Carey-Gailhardis, E. & Mercier, J.L., 1987. A numerical method for determining the state of stress using focal mechanisms of earthquake populations, *Earth planet. Sci. Lett.,* **82,** 165–179.

Carlson, R.L. & Melia, P.J.A., 1984. Subduction hinge migration, *Tectonophysics,* **102,** 399–411.

Chorowicz, J., Luxey, P., Lybéris, N., Carvalho, J., Parrot, J.F., Yürür, T. & Gündoğdu, N., 1994. The Maraş Triple Junction (southern Turkey) based on digital Elevation Model and satellite imagery interpretation, *J. geophys. Res.,* **99,** 20 225–20 242.

Chorowicz, J., Dhont, D. & Gündoğdu, N., 1999. Neotectonics in the eastern North Anatolian Fault region (Turkey) advocates crustal extension: mapping from SAR ERS imagery and Digital Elevation Model, *J. struc. Geol.,* **21,** 511–532.

Comninakis, P.E. & Papazachos, B.C., 1972. Sesimicity and some tectonic features of the Mediterranean ridge, *Geol. Soc. Am. Bull.,* **83,** 1093–1102.

DeMets, C., Gordon, R.G., Argus, D.F. & Stein, S., 1990. Current plate motions, *Geophys. J. Int.,* **101,** 425–478.

Demirtas, R. & Yilmaz, R., 1996. *Seismotectonics of Turkey: Preliminary Approach to Earthquake Forecasting Based on Long-term Variations in Seismic Activity and Present-Seismicity,* Seis. Div., Earthq. Res. Dep., Ministry of Reconstruction and Resettlement, Ankara.

Dewey, J.F., 1980. Episodicity, sequence and style at convergence plate boundaries, in *The Continental Crust and its Mineral Deposits,* ed. Strangeway, D.F., *Spec. Publ. Geol. Ass. Canada,* **20,** 553–573.

Dewey, J.F., Hempton, M.R., Kidd, W.S.F., Saroglu, F. & Sengör, A.M.C., 1986. Shortening of continental lithosphere: the neotectonics of Eastern Anatolia—a young collision zone, in *Collision Tectonics,* eds Coward, M.P. & Ries, A.C., *Geol. Soc. London, Sp. Publ.,* **19,** 3–36.

Erdik, M., Aydınoglu, N., Pınar, A. & Kalafat, D., 1997. *Hatay Deprem Raporu*, Kandilli, Obs. Istanbul.

Erentoz, C. & Pamir, H.N., 1964, *1:500.000 Geological map of Turkey*, MTA, Ankara.

Forsyth, D.W. & Uyeda, S., 1975. On the relative importance of driving forces of plate motion, *Geophys. J. R. astr. Soc.,* **43,** 163–200.

Garfunkel, Z., 1988. Relation between continental rifting and uplift: evidence from the Suez rift and northern Red Sea, *Tectonophysics,* **150,** 33–50.

Gephart, J.W. & Forsyth, D.W., 1984. An improved method for determining the regional stress tensor using earthquake focal mechanism data: an application to the San Fernando earthquake sequence, *J. geophys. Res.,* **89,** 9305–9320.

Gökçen, S.L., Kelling, G., Gökçen, N. & Floyd, P.A., 1986. Sedimentology of a Late Cenozoic collisional sequence: the Misis Complex, southern Turkey, *Sediment. Geol.,* **59,** 205–223.

Gürsoy, H., Piper, J.D.A., Tatar, O. & Mesci, L., 1998. Paleomagnetic study of the Karaman and Karapınar volcanic complex, central Turkey: Neotectonic rotation in the south central sector of the Anatolian Block, *Tectonophysics,* **299,** 191–211.

Hancock, P.L. & Barka, A.A., 1987. Kinematic indicators on active normal faults in Western Turkey, *J. Struct. Geol.,* **9,** 573–584.

Hempton, M.R., 1987. Constraints on Arabian plate motions; an extensional history of the Red sea, *Tectonics,* **6,** 668–705.

Jackson, J. & McKenzie, D.P., 1984. Active tectonics of the Alpine-Himalayan belt between western Turkey and Pakistan, *Geophys. J. R. astr. Soc.,* **77,** 185–264.

Jackson, J. & McKenzie, D.P., 1988. The relationship between plate motion and seismic moment tensors, and the rates of active deformation in the Mediterranean and Middle-East, *Geophys. J. R. astr. Soc.,* **93,** 45–73.

Kempler, D. & Garfunkel, Z., 1994. Structures and kinematics in the northeastern Mediterranean: A study of an irregular plate boundary, *Tectonophysics,* **234,** 19–32.

Kikuchi, M. & Kanamori, H., 1991. Inversion of complex body waves-II. *Bull. seism. Soc. Am.,* **81,** 2335–2350.

Le Pichon, X., 1982. Land-locked oceanic basins and continental collision: the eastern Mediterranean as a case example, in *Mountain Building Processes,* 201–211, eds Hsü, K., Academic Press, New York, NY.

Le Pichon, X. & Angelier, J., 1979. The Hellenic Arc and trench system: a key to the neotectonic evolution of the eastern Mediterranean area. *Tectonophysics,* **60,** 1–42.

Le Pichon, X. & Angelier, J., 1981. The Aegean Sea, *Phil. Trans. R. Soc., Lond.,* A., **300,** 357–372.

Lovelock, P.E.R., 1984. A review of the tectonics of the northern middle-East region, *Geol. Mag.,* **121,** 577–587.

Lyberis, N., Yurur, T., Chorowicz, J., Kasapoglu, E. & Gündogdu, N., 1992. The East Anatolian Fault: an oblique collisional belt, *Tectonophysics,* **204,** 1–15.

Markis, J., 1981. Deep structure of the eastern Mediterranean deduced from refraction seismic data (abstract), *EOS, Trans. Am. geophys. Un.,* **62,** 6247.

Malinverno, A. & Ryan, W., 1986. Extension in the Tyrrhenian Sea and shortening in the Apennines as a result of arc migration driven by sinking of the lithosphere, *Tectonics,* **5,** 227–245.

Mart, Y. & Rabinowitz, P.D., 1986. The northern Red Sea and the Dead Sea rift, *Tectonophysics,* **124,** 85–113.

Mart, Y. & Woodside, J., 1994. Preface: tectonics of the Eastern Mediterranean, *Tectonophysics,* **234,** 1–3.

McKenzie, D.P., 1972. Active tectonics of the Mediterranean Region, *Geophys. J. R. astr. Soc.,* **30,** 109–185.

McKenzie, D.P., 1978. Active tectonics of the Alpine-Himalayan belt: the Aegean sea and surrounding regions (tectonic of Aegean region), *Geophys. J. R. astr. Soc.,* **55,** 217–254.

Mercier, J.L., 1981. Extensional-compressional tectonics associated with the Aegean Arc: comparison with the Andean Cordillera of south Peru-North Belivia, *Phil. Trans. R. Soc. Lond.,* A., **300,** 337–355.

Mercier, J.L., Delibassis, N., Gauthier, A., Jarrige, J.J., Lemeille, F., Philip, H., Sébrier, M. & et Sorel, D., 1979. La néotectonique de l'Arc Egéen, *Rev. Géol. Dynam. Géogr. Phys., Paris,* **21,** 67–92.

Mercier, J.L., Sorel, D. & Vergely, P., 1989. Extensional tectonic regimes in the Aegean basins during the Cenozoic, *Basin Research,* **2,** 49–71.

Mercier, J.L., Carey-Gailhardis, E. & Sébrier, M., 1991. Paleostress determinations from fault kinematics: application to the neotectonics of the Himalayas-Tibet and the Central Andes., *Phil. Trans. R. Soc. Lond.,* A., **337,** 41–52.

Muehlberger, W.B., 1981. The splintering of the Dead Sea fault zone in Turkey, *Bull. Inst. Earth Sci. Hacetepe Univ.*, *Ankara,* **8,** 125–130.

Nowroozi, A.A., 1972. Focal mechanism of earthquakes in Persia, Turkey, West Pakistan and Afghanistan, and plate tectonics of the Middle East, *Bull. seism. Soc. Am.,* **62,** 823–850.

Nur, A. & Ben-Avraham, Z., 1978. The eastern Mediterranean and the Levant: Tectonics of continental collision, *Tectonics,* **46,** 297–311.

Osmansahin, I., Eksi, F. & Alptekin, Ö., 1986. Dogu Anadolu ve Kafkasya bölgesinin depremselligi ve aktif tektonigi, *Bull., Earthq. Res. Inst.,* Ministry of Reconstruction and Resettlement, **52,** 5–41.

Over, S., Bellier, O., Poisson, A. & Andrieux, J., 1997. Late Cenozoic stress state changes along the central North Anatolian Fault zone (Turkey), *Ann. Tectonicae,* **XI,** 75–101.

Papazachos, B.C., 1973. Distribution of seismic foci in the Mediterranean area and its tectonic implications, *Geophys, J. R. astr. Soc.,* **33,** 421–430.

Perinçek, D. & Çemen, I., 1990. The structural relationship between the East Anatolian Fault and Dead Sea Fault zones in southern Turkey, *Tectonophysics,* **172,** 331–340.

Perinçek, D. & Eren, A.G., 1990. Doğrultu atımlı Doğu Anadolu ve Ölü Deniz fay zonları etki alanında gelişen Amik havzasının kökeni, Turkiye 8. Petrol Kongresi Bildiri Kitabı, 180–192.

Poirier, J.P. & Taher, M.A., 1980. Historical seismicity in the Near and Middle East, North Africa and Spain from Arabic documents, *Bull. seism. Soc. Am.,* **70,** 2185–2201.

Rabinowitz, P.D. & Ryan, W.F.B., 1970. Gravity anomalies and crustal shortening in the eastern Mediterranean, *Tectonophysics,* **10,** 585–608.

Robertson, A.H.F., 1990. Tectonic evolution of Cyprus, in *Ophiolites and Oceanic Lithosphere,* eds Moores, E.M., *et al., Proc. Int. Symp. Nicosia,* 235–250.

Robertson, A.H.F., Eaton, S., Follows, E.J. & McCullum, J.E., 1991. The role of local tectonics versus global sea-level change in the Neogene evolution of the Cyprus active margin, *Spec. Publ. Int. Ass. Sediment,* **12,** 331–369.

Rojay, B., Heimann, A. & Toprak, V., 2001. Neotectonic and volcanic characteristics of the Karasu Fault zone (Anatolia, Turkey): The transition zone between the Dead Sea transform and the East Anatolian fault zone, *Geodinamica Acta,* **14,** 197–212.

Rotstein, Y. & Kafka, A.L., 1982. Seismotectonics of the southern boundary of Anatolia, eastern Mediterranean region: subduction, collision and arc jumping, *J. geophys. Res.,* **87,** 7694–7706.

Rotstein, Y. & Ben-Avraham, Z., 1985. Accretionary processes at subduction zones in the eastern Mediterranean, *Tectonophysics,* **112,** 551–561.

Saroğlu, F. & Yilmaz, Y., 1990. Tectonics of the Karlıova triple junction, *Bull. ITU Istanbul*.

Saroglu, F., Emre, Ö. & Kusçu, I., 1992. The East Anatolian fault zone of Turkey, *Ann. Tectonicae,* **VI,** 99–125.

Sebrier, M., Mercier, J.L., Macharé, J. Bonnot, D., Cabrera, J. & Blanc, J.L., 1988. The state of stress in an overridding plate situated above a flat slab: the Andes of central Peru, *Tectonics,* **7,** 895–928.

Sebrier, M. & Soler, P., 1991. Tectonics and Magmatism in the Peruvian Andes from late Oligocene time to Present, *Geol. Soc. Am. Spec. Paper,* **265,** 259–277.

Sengör, A.M.C., 1979. The North Anatolian transform fault: its age, offset and tectonic significance, *J. geol. Soc. Lond.,* **136,** 269–282.

Sengör, A.M.C., Görür, N. & Saroglu, F., 1985. Strike-slip faulting and related basin formation in zones of tectonic escape: Turkey as a case

study, in *Strike-slip Deformation,* eds Biddle, K.T. & Christie-Blick, N., Basin Formation and Sedimentation, *Soc. Econ. Paleont. Mineral. Tulsa, Sp. Publ.,* **37,** 227–264.

Sorel, D., Mercier, J.L., Keraudren, B. & Cushing, M., 1988. Le role de la traction de la lithosphere subducté dans l'évolution géodynamique Plio-Pleistocene de l'Arc Egéen: mouvement verticaux alternés et variations du régime tectonique, *C. R. Acad. Sci., Paris,* **307,** 1981–1986.

Tapponnier, P., 1977. Evolution tectonique du systeme alpine en Méditerranée: Poincement et ecrasement rigide-plastique, *Bull. Soc. Geol., Fr.,* **7,** 437–460.

Taymaz, T., Eyidoğan, H. & Jackson, J., 1991. Source parameters of large earthquakes in the East Anatolian Fault Zone (Turkey), *Geophys. J. Int.,* **106,** 537–550.

Vasseur, G., Etchecopar, A. & Philip, H., 1983. Stress state inferred from multiple focal mechanisms, *Ann. Geophys.,* **1,** 291–298.

Westaway, R., 1994. Present-day kinematics of the Middle East and eastern Mediterranean, *J. geophys. Res.,* **99,** 12 071–12 090.

Westaway, R. & Arger, J., 1996. The Gölbaşı basin, southeastern Turkey: a complex discontinuity in a major strike-slip fault zone, *J. geol. Soc. Lond.,* **153,** 729–744.

Yürür, T. & Chorowicz, J., 1998. Recent volcanism, tectonics and plate kinematics near the junction of African, Arabian and Anatolian plates in the eastern Mediterranean, *J. Volc. Geotherm. Res.,* **85,** 1–15.

Zanchi, A., & Angelier, J., 1993. Seismotectonics of western Anatolia: regional stress orientation from geophysical and geological data, *Tectonophysics,* **222,** 259–274.

Zoback, M.L. & Zoback, M.D., 1980. State of stress in the conterminous United states, *J. geophys. Res.,* **85,** 6113–6156.

APPENDIX 1

Table A1. Location of fault striae measurement sites with latitude (lat.), longitude (long.) and age of faulted formations. Eo: Eocene, M: Miocene, Pl: Pliocene, Q: Quaternary (Erentöz & Pamir 1964).

Sites	Lat. (N)	Long. (E)	Age
1	36°07.2′	35°97.8′	Pl-Q
2	36°12.1′	36°01.8′	Pl-Q
3	36°14.3′	36°06.0′	Pl-Q
4	36°15.2′	36°07.2′	Pl-Q
5	36°17.5′	36°10.1′	Pl-Q
6	36°18.0′	36°11.3′	M-Pl
7	36°13.4′	36°14.2′	M-Pl
8	36°19.2′	36°19.1′	Eo
9	36°20.2′	36°17.3′	Eo
10	36°20.8′	36°17.7′	Eo
11	36°22.1′	36°18.1′	Eo
12	36°22.3′	36°20.2′	M
13	36°23.0′	36°20.9′	M
14	36°39.5′	36°25.3′	Eo
15	36°40.2′	36°25.8′	Eo
16	36°41.1′	36°26.3′	Eo
17	36°41.3′	36°26.4′	Eo
18	36°45.2′	36°27.0′	M
19	36°48.4′	36°29.2′	M
20	36°47.8′	36°32.2′	M
21	36°47.7′	36°32.6′	Eo
22	36°47.3′	36°26.1′	Eo
23	36°47.8′	36°23.5′	Eo
24	36°48.3′	36°22.3′	M
25	36°48.1′	36°20.2′	Eo
26	36°48.2′	36°19.9′	M

APPENDIX 2

Table A1. Results of stress tensor inversions for slip data representing strike-slip faulting stress regimes. In the site column '&' indicates an inversion solution computed from two data sets from different sites; for example 11 & 12 correspond to an inversion computed from the data sets of sites 11 and 12. N = number of striated fault planes used to compute the solutions. SFmaj1 is an average and stable stress state obtained by inversion of major and/or representative fault planes selected from each kinematics site. '$*$' indicates a 'fixed inversion' (stress axes constrained to lie in horizontal and vertical planes). The mean deviation of the deviation angle is 'M.D.' $= [\Sigma(\tau, s)^2]/N$, where (τ, s) is the angle between the predicted slip vector, t, and observed slip vector s. The standard deviation of the deviation angle is 'S.D.' $= \{[\sigma(\tau, s)^2]/N\}^{1/2}$.

Sites	N	σ_1 Az/dip	σ_2 Az/dip	σ_3 Az/dip	R	M.D.	S.D.
1	17	168/32	342/58	76/23	0.63	6.7	8.2
1*		169/0	14/90	259/0	0.41	11.3	15.8
2	11	331/29	139/60	239/6	0.04	5.7	5.6
2*		157/1	338/89	247/0	0.04	10.1	12.8
3	10	305/7	135/83	35/1	0.88	8.7	10.7
3*		136/0	272/90	259/0	0.82	7.9	12.6
4 & 5	18	316/16	110/72	224/8	0.41	8.3	12.8
4 & 5*		147/0	330/90	232/0	0.54	12.4	17.7
6	25	143/8	310/82	53/2	0.85	11.0	14.4
7	13	326/12	127/77	236/4	0.83	6.2	9.1
11 & 12	16	123/9	242/73	30/15	0.94	10.7	13.8
13	12	173/6	289/77	81/12	0.47	11.3	12.8
14–17	21	328/16	165/73	59/5	0.13	13.5	15.6
18	15	353/10	177/80	83/1	0.33	9.9	12.4
19	10	135/7	309/83	45/1	0.32	9.5	11.3
20 & 21	11	133/9	156/81	63/0	0.05	9.7	11.6
23 & 24	30	330/6	193/82	60/6	0.91	13.9	16.3
25 & 26	15	297/2	40/80	207/10	0.54	8.1	9.8
SFmaj1	18	$\sigma_1 = 326°/9°$	and	$\sigma_3 = 56/1°$	$R = 0.30$		

Table A2. (a) Results of stress tensor inversions for slip data representing NE-trending normal faulting stress regimes. In the site column '-' indicates an inversion solution computed from more than two data sets at different close sites; for example, 14–17 corresponds to an inversion computed from small data sets from the close sites 14, 15, 16 and 17. SFmaj2 is an average and stable stress state obtained by inversion of major and/or representative fault planes selected from each kinematics site. Sfm is the regional stress state for same tectonic regime obtained from focal mechanism inversions. (b) Results of local stress tensor inversions for seismic fault-slip data representing local normal faulting stress regime with strike-slip component.

Sites	N	σ_1 Az/dip	σ_2 Az/dip	σ_3 Az/dip	R	M.D.	S.D.
(a)							
3				ENE-WSW			
4 & 6	11	129/80	325/10	234/3	0.84	8.9	9.8
8 & 9a	13	201/88	306/1	36/2	0.67	12.9	15.1
10	11	123/60	314/29	221/5	0.60	11.7	14.4
10*		127/90	298/0	28/0	0.51	14.4	18.3
11 & 12a	16	123/71	296/19	27/2	0.60	11.2	14.2
14–17	13	85/79	337/3	247/10	0.53	9.0	11.8
22 & 23	10	217/62	325/9	59/26	0.99	7.3	10.8
22 & 23*		128/90	294/0	24/0	0.66	8.3	13.9
SFmaj2	10	$\sigma_2 = 308/0°$	and	$\sigma_3 = 218/4°$	$R = 0.63$		
Sfm	9	$\sigma_2 = 327/13°$	and	$\sigma_3 = 51/1°$	$R = 0.21$		
(b)							
8 & 9b	9	316/73	208/5	117/16	0.75	3.9	4.9
8 & 9b*		136/90	294/0	282/0	0.96	5.6	6.9
11 & 12b	5			ENE-WSW			